HHS Public Access

Author manuscript

Nat Cell Biol. Author manuscript; available in PMC 2016 May 01.

Published in final edited form as:

Nat Cell Biol. 2015 November ; 17(11): 1401–1411. doi:10.1038/ncb3258.

Heterochromatic breaks move to the nuclear periphery to continue recombinational repair

Taehyun Ryu[1], **Brett Spatola**[1], **Laetitia Delabaere**[1], **Katherine Bowlin**[1], **Hannah Hopp**[1], **Ryan Kunitake**[2], **Gary H. Karpen**[2,3], and **Irene Chiolo**[1,*]

[1]University of Southern California, Molecular and Computational Biology Department, 90089, Los Angeles, California

[2]Lawrence Berkeley National Laboratory, Genome Dynamics Department, 94720, Berkeley, California

[3]University of California Berkeley, Molecular and Cell Biology Department, 94720, Berkeley, California

Abstract

Heterochromatin mostly comprises repeated sequences prone to harmful ectopic recombination during double-strand break (DSB) repair. In *Drosophila* cells, 'safe' homologous recombination (HR) repair of heterochromatic breaks relies on a specialized pathway that relocalizes damaged sequences away from the heterochromatin domain before strand invasion. Here we show that heterochromatic DSBs move to the nuclear periphery to continue HR repair. Relocalization depends on nuclear pore and inner nuclear membrane proteins (INMPs) that anchor repair sites to the nuclear periphery *via* the Smc5/6-interacting proteins STUbL/RENi. Both the initial block to HR progression inside the heterochromatin domain, and the targeting of repair sites to the nuclear periphery, rely on SUMO and SUMO E3 ligases. This study reveals a critical role for SUMOylation in the spatial and temporal regulation of HR repair in heterochromatin, and identifies the nuclear periphery as a specialized site for heterochromatin repair in a multicellular eukaryote.

Nuclear architecture contributes to HR repair of certain types of DSBs in budding yeast. Specifically, most DSBs exhibit Brownian motion and remain in the nucleoplasm during HR[1–4], but persistent DSBs are shunted to the nuclear periphery after resection[1,2,5,6]. This relocalization has been observed in conditions where HR repair is effectively stalled, such as

---

*Correspondence should be addressed to: chiolo@usc.edu.

Competing financial interests

The authors declare no competing financial interests.

Author Contributions

T.R. performed most experiments. B.S. performed experiments for Figs 5f and 6a and helped executing RNAi, IF, and imaging experiments. L.D. performed experiments for Fig. 6e. K.B. performed qPCR analyses. H.H. generated the script for MSD analyses. R.K. performed experiments for Supplementary Fig. 1a, RNAi validations, and CoIP optimizations. T.R., B.S. and L.D. contributed to manuscript preparation. G.K. contributed to project planning, experimental design, and manuscript preparation. I.C. contributed to project planning, experimental design and execution, and manuscript preparation.

in the absence of a donor sequence for repair[1,2,5,6] or after fork collapse[1,7]. Whether relocalization is a physiological response to DSBs is still controversial, and the existence of similar roles for the nuclear periphery in multicellular eukaryotes has not been addressed.

Pericentromeric heterochromatin occupies about 30% of fly and human genomes[8] and is characterized by large contiguous stretches of repeated sequences (transposons and 'satellite' repeats[9–11]) and the 'silent' epigenetic marks H3K9me2/3 and Heterochromatin Protein 1 (HP1a in *Drosophila*)[12]. While pericentromeric heterochromatin is absent in budding yeast, it represents a major threat to genome stability in multicellular eukaryotes[13,14]. Thousands to millions of identical repeated sequences on different chromosomes can engage in ectopic recombination and generate chromosome rearrangements[13,14] (*e.g.*, acentric and dicentric chromosomes) during DSB repair. We previously identified a mechanism that promotes HR repair while preventing aberrant recombination in *Drosophila*[14,15]. Early HR steps (resection and ATRIP/TopBP1 recruitment) occur quickly within the heterochromatin domain[15], but later steps (Rad51 recruitment) occur only after repair sites have relocalized to outside the domain[15,16]. Relocalization of heterochromatic DSBs also occurs in mouse cells, suggesting that this mechanism is conserved[14,17]. We proposed that relocalization prevents aberrant recombination by separating damaged DNA from similar repeats on non-homologous chromosomes, while promoting 'safe' exchanges with the sister chromatid or homolog[14,15]. Removing heterochromatic proteins (*e.g.*, Smc5/6) results in relocalization defects, abnormal recruitment of Rad51 inside the heterochromatin domain, and massive aberrant recombination between heterochromatic sequences[15], revealing the importance of this pathway to genome stability. Whether heterochromatic DSBs relocalize to a specific subnuclear compartment was unclear, and the mechanisms responsible for relocalization and the regulation of HR progression were unknown.

RESULTS

SUMOylation blocks HR progression in heterochromatin and promotes DSB relocalization

In *S. cerevisiae*, SUMOylation mediates the relocalization of DSBs in ribosomal DNA (rDNA) to outside the nucleolus[18] and the movement of persistent DSBs to the nuclear periphery[6]. The Smc5/6 complex is required for relocalizing heterochromatic DSBs in *Drosophila*[15] and contains the SUMO E3 ligase Nse2[19–21], leading us to investigate the role of SUMOylation and SUMO ligases in heterochromatin repair. First, we determined that SUMO ligases are present at heterochromatic DSBs by monitoring the recruitment of these proteins to repair foci induced by ionizing radiation (IR). Nse2 is broadly enriched in the heterochromatin domain in the absence of IR[15] (Fig. 1a). However, shortly after IR and similar to other early repair components (*e.g.*, TopBP1/ATRIP[15]), Nse2 is recruited to foci inside the heterochromatin domain that colocalize with the DSB markers γH2Av and TopBP1 (Figs. 1a,b and Supplementary Fig. 1a). Other Smc5/6 subunits form foci with similar kinetics (Supplementary Fig. 1b), and Nse2 focus formation depends on the core subunits Smc5 and Smc6 (Supplementary Fig. 1c), suggesting that Nse2 is recruited to heterochromatic DSBs as part of the Smc5/6 complex. Yeast Nse2/Mms21 shares numerous targets with the SUMO E3 ligases Siz1 and Siz2[22–25], homologs of *Drosophila* dPIAS[26].

dPIAS is also recruited to heterochromatic repair foci with kinetics similar to ATRIP/TopBP1 (Fig. 1c and[15]). Bright dPIAS foci frequently overlap with dim γH2Av foci, and *vice versa* (Fig. 1c), and the peak of dPIAS focus intensity temporally precedes that of γH2Av (Supplementary Fig. 1d), suggesting that dPIAS recruitment to DSBs precedes γH2Av spreading. These data suggest an early function of Nse2 and dPIAS SUMO ligases at heterochromatic DSBs.

We then examined the roles of Nse2, dPIAS and SUMOylation in DSB relocalization. Most DSBs move to outside the heterochromatin domain between 10 and 30 min after IR[15], resulting in a low number of γH2Av foci inside the domain at later times[15]. Defective relocalization, *e.g.* after Smc5/6 depletion by RNAi, results in higher numbers of γH2Av foci inside the domain at 60 min after IR[15] (Fig. 1d), without affecting the total number of repair foci[15] (Supplementary Fig. 1f). We observed similar effects after Nse2 or dPIAS RNAi (Fig. 1d and Supplementary Fig. 1f), while Smc5/6 recruitment to heterochromatin and damage foci is unaffected in these conditions (Supplementary Fig. 1j). Simultaneous depletion of Nse2 (or Smc5/6) and dPIAS results in additive effects, *i.e.* higher numbers of γH2Av foci retained in the heterochromatin domain compared to each individual RNAi (Fig. 1d and Supplementary Fig. 1f), and the magnitude of this effect resembles that of SUMO RNAi (Fig. 1d and Supplementary Fig. 1f). We conclude that relocalization of heterochromatic DSBs requires SUMOylation and is mediated by the partially-redundant SUMO ligases Nse2 and dPIAS.

Next, we investigated whether SUMOylation also contributes to preventing HR progression and aberrant recombination in heterochromatin. Rad51 mediates the strand invasion step of HR, and Rad51 foci form at heterochromatic DSBs only after repair sites have relocalized to outside the domain[15]. Similar to Smc5/6 RNAi[15], Nse2 or dPIAS RNAi results in abnormal formation of Rad51 foci inside the heterochromatin domain at 60 min after IR, without affecting the total number of Rad51 foci (Fig. 1e and Supplementary Fig. 1k). RNAi depletion of Nse2+dPIAS has additive effects, resulting in levels of Rad51 foci in heterochromatin equivalent to SUMO RNAi (Fig. 1e and Supplementary Fig. 1k). In addition, similar to Smc5/6 RNAi[15], Nse2 and dPIAS RNAi results in formation of Rad51-dependent heterochromatic DNA filaments between dividing cells (Fig. 1f), reflecting aberrant recombination between repeated sequences[15]. We conclude that SUMOylation by Nse2 and dPIAS prevents Rad51 recruitment to heterochromatic DSBs and aberrant recombination in heterochromatin, in addition to promoting DSB relocalization.

STUbL/RENi proteins work with Smc5/6 to relocalize heterochromatic DSBs

Several HR components are SUMOylated during repair[23,24,27], and they might promote DSB relocalization by interacting with SUMO-binding components outside the heterochromatin domain[28]. Candidates for this function are SUMO-targeted ubiquitin ligases (STUbLs) that regulate HR progression in yeast and mammalian cells[1,2,7,29–31]. STUbLs are functionally related to RENi family proteins (Rad60/Esc2/Nip45 homologs)[32,33], which contain SUMO-like domains interacting with STUbLs[32,34,35]. While the role of RENi proteins is still enigmatic, the *S. pombe* RENi/Rad60 protein is also a known Smc5/6 interactor[36].

RNAi depletion of *Drosophila* STUbL/Dgrn[37] or RENi/CG44490[34] (hereafter dRad60) results in persistent γH2Av foci in heterochromatin (Fig. 2a), without affecting the kinetics of euchromatic foci, or the total number of foci (Fig. 2a). This reveals a role for Dgrn/dRad60 in heterochromatic DSB relocalization. Epistasis analysis indicates that Dgrn, dRad60 and Smc5/6 regulate heterochromatin DSB relocalization through the same pathway: individual depletions produced levels of persistent heterochromatic γH2Av foci similar to Dgrn+dRad60 or Dgrn+dRad60+Smc5/6 RNAi (Fig. 2b and Supplementary Fig. 2c,d). Importantly, neither Dgrn nor Rad60 RNAi affects Smc6 or Nse2 recruitment to heterochromatin and repair foci (Supplementary Fig. 2e), indicating that Dgrn/dRad60 act downstream of Smc5/6 to promote DSB relocalization. Interestingly, Dgrn and dRad60 constitutively interact (Fig. 2c), but only associate with Smc5/6 in response to IR (Fig. 2d). dRad60 RNAi does not affect Smc5/6-Dgrn interactions (Supplementary Fig. 2g), suggesting that dRad60 is not an Smc5/6-Dgrn 'adapter' and may instead regulate Dgrn activity[25,38,39]. We conclude that Dgrn and dRad60 regulate DSB relocalization downstream of Smc5/6, likely by promoting Dgrn/dRad60 interactions with Smc5/6 and/or its SUMOylated targets.

Yeast STUbL and RENi proteins prevent aberrant recombination[1,7,40–42] and regulate the levels of Nse2 SUMOylation targets[25], suggesting that Drosophila STUbL/RENi could contribute to preventing Rad51 recruitment inside the heterochromatin domain. However, unlike Nse2 and/or dPIAS RNAi, neither Dgrn nor dRad60 RNAi induces abnormal recruitment of Rad51 within the heterochromatin domain, or generates heterochromatic DNA filaments between dividing cells (Figs 2e,f and Supplementary Fig. 2h).

We conclude that the block to HR progression inside the heterochromatin domain and DSB relocalization to outside the domain are genetically separable pathways; SUMOylation is required for both, but STUbL and RENi proteins only contribute to relocalization. Identification of this role for Dgrn and dRad60 prompted us to search for other components specifically involved in relocalization. Intriguingly, Dgrn and dRad60 are enriched at the nuclear periphery (Fig. 2g), with dRad60 peripheral localization depending on Dgrn (Fig. 2h). This localization of Dgrn/dRad60 suggests a role for the nuclear periphery in relocalizing heterochromatic DSBs.

Nuclear pores and INMPs are required for relocalizing heterochromatic DSBs

In *S. cerevisiae*, association of persistent DSBs with the nuclear periphery is mediated by nuclear pores[1,5,6] or the SUN domain protein Mps3[2,5,6]. Destabilizing *Drosophila* nuclear pores by Nup153 RNAi[43] results in persistent γH2Av foci in heterochromatin (Supplementary Fig. 3b,c), indicating a role for nuclear pores in relocalizing heterochromatic DSBs. To identify specific components involved, we RNAi depleted other pore subunits not essential for pore integrity (Supplementary Fig. 3b and and[43]), focusing on sub-complexes facing the nuclear interior that are more likely to interact with chromatin (Fig. 3a). Relocalization defects were observed after RNAi depletion of the outer ring subunits Nup107 or Nup160 (Figs 3b,c and Supplementary Figs 3d,e), but not after depletion of other basket components, inner ring subunits, and linker Nups (Fig. 3c and Supplementary Figs 3d,e). We conclude that the pore outer ring is specifically required for

relocalizing heterochromatic DSBs. Notably, the Nup107-160 complex is not required for transport through pores[43], suggesting that the observed relocalization defects are not due to defective transport.

Next, we investigated the role of INMPs, specifically the *Drosophila* Mps3 homologs Koi and Spag4[44]. Koi+Spag4 RNAi results in persistent γH2Av foci in heterochromatin (Fig. 3d and Supplementary Fig. 3f); both Koi and Spag4 are independently required for relocalizing heterochromatic foci, with Spag4 RNAi resulting in a slightly stronger relocalization defect compared to Koi RNAi (Fig. 3e and Supplementary Fig. 3g). Simultaneous RNAi depletion of these INMPs together with Nup107 or Nup153 has an additive effect relative to individual RNAi depletions, or Koi+Spag4 RNAi (Fig. 3e and Supplementary Fig. 3g). Additionally, Smc5/6 RNAi does not aggravate the relocalization defect observed after Nup107+Koi+Spag4 RNAi (Fig. 3f and Supplementary Figs 3h,i). We conclude that both nuclear pores and INMPs work in concert with Smc5/6, but independently from each other, in relocalizing heterochromatic DSBs.

Nuclear pores and INMPs recruit STUbL/RENi to the nuclear periphery and work with STUbL/RENi for DSB relocalization

Nuclear pores and INMPs are mostly associated with the nuclear periphery, similar to Dgrn/dRad60, and could mediate the recruitment of these STUbL/RENi components to the periphery. We first determined if Dgrn and dRad60 colocalize with nuclear pores and/or INMPs. Nuclear pores, Koi and Spag4 largely colocalize at the resolution of wide-field fluorescence microscopy, but form separate clusters after Lamin RNAi (Fig. 4a and[45]). Koi colocalizes with Lamin clusters, while Spag4 colocalizes with nuclear pore clusters (Supplementary Fig. 4b). Dgrn and dRad60 colocalize with both Koi and nuclear pore/Spag4 clusters (Fig. 4b), suggesting that STUbL/RENi are associated with both nuclear pores and INMPs at the nuclear periphery.

Next, we investigated the role of nuclear pores and INMPs in recruiting STUbL/RENi proteins. Simultaneous RNAi depletion of Nup107, Koi and Spag4 results in complete loss of Dgrn and dRad60 at the nuclear periphery (Fig. 4c), without affecting Dgrn/dRad60 protein levels (Supplementary Fig. 4c). We noticed that RNAi depletion of Nup107 alone, or Koi+Spag4, has partial effects (Supplementary Fig. 4d), indicating that nuclear pores and INMPs are partially redundant for Dgrn/dRad60 recruitment. Notably, Nup153 is still associated with the pores after depletion of Nup107+Koi+Spag4 (Supplementary Fig. 4e), yet Dgrn/dRad60 are dissociated from the nuclear periphery, indicating that Nup153 is not sufficient to tether Dgrn/dRad60 to the pores. Thus, the pore outer ring, and Koi and Spag4 INMPs, act as specific and independent anchoring sites for STUbL/RENi at the nuclear periphery.

Similar to STUbL/RENi, Nup107 and INMPs are required for relocalizing heterochromatic repair foci (Fig. 3), but not for blocking Rad51 recruitment inside the heterochromatin domain: RNAi depletion of nuclear pore components and INMPs does not result in Rad51 foci inside the heterochromatin domain after IR, or formation of heterochromatic DNA filaments connecting dividing cells (Supplementary Figs 4f,g). Additionally, neither Dgrn nor dRad60 RNAi aggravates the relocalization defect observed after Nup107+Koi+Spag4

RNAi (Fig. 4d and Supplementary Fig. 4h). We conclude that nuclear pores and INMPs work in the same pathway as Dgrn/dRad60 to promote relocalization of heterochromatic DSBs, likely by anchoring Dgrn/dRad60 to the nuclear membrane.

Heterochromatic DSBs relocalize to the nuclear periphery

The importance of nuclear membrane-associated proteins in relocalizing heterochromatic DSBs suggests that heterochromatic repair foci relocalize to the nuclear periphery during repair. However, INMPs and outer ring pore subunits also play independent roles in the nucleoplasm[46–49], requiring more direct evaluation of the role of the nuclear periphery in relocalization. First, we observed that repair foci become enriched at the nuclear periphery between 10 and 60 min after IR, concurrent with relocalization of heterochromatic DSBs away from the heterochromatin domain[15] (Fig. 5a and Supplementary Fig. 5a). Preventing relocalization of heterochromatic DSBs by HP1a or Smc5/6 RNAi[15] drastically reduces the number of repair foci at the nuclear periphery (Fig. 5b and Supplementary Fig. 5c), to levels observed in the absence of IR (Fig. 5a). Strikingly, this suggests that most DSBs associated with the nuclear periphery at 60 min after IR are heterochromatic, which was confirmed by observing that nearly 80% of repair sites associated with the nuclear periphery are enriched for H3K9me2/3 (Fig. 5c). These DSBs are mostly localized at the tips of protrusions extending from the main bulk of the heterochromatic domain (Fig. 5c), which form when DSBs relocalize[15]. At the nuclear periphery, γH2Av foci largely colocalize with Rad51 and Brca2 (a mediator of Rad51 recruitment[50,51]) (Fig. 5d), and Mu2/Mdc1 (a γH2Av-binding protein[15,52]) colocalizes with Rad51 (Supplementary Fig. 5d), suggesting that HR repair progresses at these sites.

Second, association of DSBs with the nuclear periphery requires nuclear pores and INMPs. Nup107+Koi+Spag4 RNAi drastically reduces the number of repair foci at the nuclear periphery (Fig. 5b) without affecting the total number of repair foci (Supplementary Fig. 5c). This effect is more pronounced than after Nup107 or Koi+Spag4 RNAi (Fig. 5b and Supplementary Fig. 5c), indicating that nuclear pores and INMPs independently recruit heterochromatic DSBs to the nuclear periphery. Accordingly, repair foci associated with the nuclear periphery colocalize with both nuclear pore and INMP clusters (Fig. 5e). Epistasis analysis demonstrates that HP1a, Smc5/6 and Dgrn work in the same pathway as Nup107+Koi+Spag4 to promote relocalization of DSBs to the nuclear periphery (Fig. 5b and Supplementary Fig. 5c). Because Nup107, Koi and Spag4 anchor Dgrn/dRad60 to the nuclear periphery, we conclude that nuclear pores and INMPs mediate the relocalization of heterochromatic DSBs to the nuclear periphery *via* STUbL/RENi.

Nup107, Koi and Spag4 may promote relocalization by anchoring heterochromatic repair sites to the nuclear periphery after they leave the heterochromatin domain. If true, the movement of heterochromatic repair foci should be less constrained and cover a larger volume in the absence of anchoring components. Live imaging of GFP-Mu2/Mdc1 foci and mean square displacement (MSD) analysis[3,4] revealed that Nup107+Koi+Spag4 RNAi leads to increased dynamics of foci that exit the heterochromatin domain (*i.e.*, larger volume explored, Fig. 5f). This indicates that nuclear pore and INMPs limit the movement of heterochromatic repair sites by tethering repair sites to the nuclear periphery.

Finally, we confirmed that heterochromatic DSBs move to the nuclear periphery by measuring the distance between heterochromatic satellite repeats and the nuclear periphery before and after IR. Damaged AACAC repeats (AACAC signals[15] colocalizing with γH2Av foci) become progressively closer to the nuclear periphery between 10 and 60 min after IR, while the distance for undamaged repeats does not change (Fig. 5g). Interestingly, AACAC satellites colocalizing with Rad51 foci are always adjacent to the nuclear periphery (Fig. 5g), suggesting that relocalization precedes Rad51 loading. We conclude that damaged heterochromatic repeats relocalize to the nuclear periphery, where Rad51 is recruited.

Relocalization is required for heterochromatin repair and stability

We directly tested the hypothesis that nuclear periphery association is a prerequisite for Rad51 recruitment to heterochromatic DSBs using live imaging of ATRIP foci, whose intensity decreases during Rad51 recruitment[15]. ATRIP focus intensity remains constant inside the heterochromatin domain and during relocalization, but significantly decreases at the nuclear periphery (Fig. 6a). Further, Nup107+Koi+Spag4 RNAi causes loss of peripheral association and a progressive increase in ATRIP focus intensity (Fig. 6a), which could result from extensive resection[53,54] and/or prolonged checkpoint signaling[55,56] when repair is halted. We conclude that nuclear periphery anchoring is required for ATRIP displacement from heterochromatic DSBs and HR progression.

These results uncover the importance of DSB relocalization in heterochromatin HR progression, but do not reveal if the relocalization pathway is essential for completing repair or other repair pathways take over in its absence. We addressed this question by determining the consequences of defective relocalization for DNA repair and genome stability. First, Nup107+Koi+Spag4 RNAi results in accumulation of γH2Av foci associated with the heterochromatin domain over time. Most foci are still present in heterochromatin 20 h after IR, a timepoint when γH2Av foci are largely resolved in control cells and in the euchromatic space of Nup107+Koi+Spag4-depleted cells (Fig. 6b and Supplementary Fig. 6b). Persistent heterochromatic γH2Av foci extensively colocalize with TUNEL signals (Supplementary Fig. 6c), suggesting that they represent unrepaired breaks. Consistent with a repair defect, RNAi depletion of relocalization components (*i.e.*, Nup107+Koi+Spag4, dRad60+Dgrn, Nse2+dPIAS, or Smc5/6) also reduces cell survival after IR exposure (Fig. 6c and Supplementary Fig. 6d). We conclude that relocalization of heterochromatic DSBs to the nuclear periphery is critical for timely completion of repair and cell viability after damage.

Second, inactivation of the relocalization pathway triggers the formation of IR-induced micronuclei containing heterochromatin marks (Fig. 6d and Supplementary Fig. 6e). Most micronuclei are not labeled by nuclear pore markers, suggesting that they represent ‘disrupted micronuclei’[57] (Fig. 6d). Micronuclei result from chromosome missegregation[58], and are a hallmark of repair defects and genome instability in cancer cells[57]. This phenotype further demonstrates the importance of DSB relocalization for heterochromatin repair and stability.

Finally, fly mutants lacking relocalization components display significant genome instability in larval neuroblasts, including aneuploidy, chromosome fusions, and changes in the number of satellites (Fig. 6e). Most fusions and aneuploidies involve the predominantly

heterochromatic 4th and Y chromosomes, or regions proximal to the centromere (Supplementary Fig. 6g), as expected for defective heterochromatin repair. These phenotypes are observed without IR, likely caused by defective repair of spontaneous DSBs that form during cell divisions in larval development. We conclude that DSB relocalization to the nuclear periphery is critical for heterochromatic DNA repair and stability, and for maintaining genome integrity, in both cultured cells and dividing tissues of the organism.

DISCUSSION

These studies reveal the nuclear periphery as a specialized site for repairing heterochromatic DSBs in *Drosophila* (Fig. 7). DSBs leave the heterochromatin domain and relocalize to nuclear pores or INMPs to continue HR repair, and this process is mediated by STUbL/RENi proteins associated with these nuclear periphery components. We identified the Nup107-160 sub-complex and Koi and Spag4 INMPs as specific anchoring sites for the STUbL/RENi complex Dgrn/dRad60 and for repair sites. Further, recruitment of dRad60 to the nuclear periphery relies on Dgrn, and both physically associate with Smc5/6 in response to damage. This suggests that interactions between Smc5/6 and Dgrn/dRad60 stabilize the association of heterochromatic DSBs with the nuclear periphery. Finally, Nse2 and dPIAS SUMO ligases and SUMO are required for both relocalizing DSBs and preventing Rad51 recruitment inside the heterochromatin domain.

We propose that SUMOylation of one or more HR components after resection, generates a temporary block to Rad51 recruitment inside the heterochromatin domain to prevent ectopic recombination. Relocalization to the nuclear periphery isolates the broken DNA, presumably together with its homologous template (sister chromatid and/or homolog) to complete ‘safe’ repair. STUbL might mediate the removal of this block by ubiquitylating poly-SUMOylated components[59], and inducing their proteasome-mediated degradation[32,35,60,61] or recognition by other repair proteins[62]. Potential SUMOylated targets include histones[6,63], RPA[29,30], Mdc1/Mu2[30], Smc5/6 subunits[23,25], Blm[64,65], and other repair[7,23–25] and heterochromatin[66,67] components. Inactivation of this pathway causes instability of repeated sequences and chromosome aberrations, revealing its critical role in heterochromatin repair and genome integrity. Importantly, inactivation of this pathway also leads to disrupted micronuclei, potentially contributing to DNA damage and genome instability in cancer cells[57].

Aspects of this pathway are surprisingly similar to the mechanism that targets persistent DSBs to the nuclear periphery in *S. cerevisiae*[1,2,5,6], including the role of Smc5/6 and SUMO (Horigome C., Gasser S.M. and colleagues, personal communication). This likely results from common signaling mechanisms, such as SUMOylation of repair components following extensive resection[1,6,54,24]. However, this similarity is unexpected because budding yeast lacks the long stretches of pericentromeric repeats that present a major challenge for DSB repair in *Drosophila* and human cells, as well as H3K9 methylation and HP1 proteins that are required for spatial and temporal regulation of heterochromatic HR repair[15]. Remarkably, a pathway utilized by yeast to deal with a rare class of ‘persistent’ DSBs[1,2,5,6], collapsed forks[1,7], or eroded telomeres[68], is now emerging as one of the most important mechanisms to safeguard genome stability in multicellular eukaryotes.

METHODS

Cell Culture

Kc167 (Kc) cells were used for all experiments and were maintained as logarithmically growing cultures in Schneider's medium (Sigma) + FBS (Gemini). Kc cells were authenticated by the *Drosophila* Genomic Resource Center (DGRC) and no mycoplasma contamination was detected[71].

IR Treatments

Cultures were exposed to IR using a 160 kV X-ray source (X-RAD iR-160, Precision X-Ray). We use a range of Gy at which the damage response (estimated based on the number of γH2Av foci) increases linearly with dose, and corresponds to nearly sublethal doses for controls (more than 90% survival at 2.5–10 Gy, Fig. 6c). A dose of 5 Gy was used for most experiments, unless otherwise indicated. The estimated number of DSBs induced by 5 Gy in *Drosophila* cells is approximately 7.5 DSBs in G1 and 14 DSBs in G2, which is based on published estimates of DSB numbers in mammalian cells[72], and the current estimates of genome sizes for human vs Drosophila cells. In kinetic analyses of fixed cells, time 0 (Unt) corresponds to cells fixed without exposure to IR. In time-lapse experiments, time 0 (Unt) corresponds to cells imaged 5–10 min before IR treatment.

Generation of cell lines expressing tagged proteins

Stable lines were obtained by cotransfecting the plasmid of interest with pCoHygro (Invitrogen) or pCoPuro (Addgene) and selecting in the presence of 100 μg/ml hygromycin B (Invitrogen) or 2 mg/ml puromycin (Enzo Life Sciences). Transfection was performed with DOTAP (Roche) or Cellfectin (Life Technologies), according to manufacturers' procedures.

Plasmids

pCopia-GFP-Mu2/Mdc1, pCopia-mCherry-HP1a, pCopia-GFP-Smc5, pCopia-GFP-Nse6 and pCopia-GFP-Nse2 plasmids were previously described[15]. With the exception of Brca2, all other GFP- and FHA-tagged proteins were generated by insertion of PCR-amplified coding regions of cDNAs from DGRC. Clone numbers were: Nse1 (GM14348), Nse3 (RE25453), Nse4 (IP09347), Dgrn (GM01182), dRad60 (RE23302), Spag4 (IP10153), and LaminC (LD31805). Detailed information is available on the DGRC web site (dgrc.cgb.indiana.edu). Brca2 was PCR amplified from pAc5.1-HA-dmBrca2[50] (gift from A. Ashworth). All PCR products were cloned into AscI/PacI-digested pCopia-LAP-EGFP vectors[73], or pCopia-3XFLAG-StrepII-HA vectors[15].

dsRNA synthesis and sequences

dsRNAs were prepared with the MEGAscript T7 Kit (Applied Biosystems). Amplicons for Bw, Smc5, Smc6, Rad51 and HP1a were previously described[15]. Amplicons used for all other dsRNAs were: DRSC04980/DRSC04991 for Koi; DRSC02973 for Spag4; DRSC01999/DRSC39982 for Nup107, DRSC07721/DRSC28335 for dPIAS; DRSC12154/DRSC38144 for Dgrn; DRSC15580 for dRad60, DRSC03359/DRSC28152 for Lamin/

DmO, DRSC19904/DRSC32510 for Nup153; DRSC03611/DRSC38466 for SUMO; DRSC05958/DRSC39824 for Mtor; DRSC01997/DRSC02774 for Nup160; DRSC19432/DRSC32817 for Nup205, DRSC16221/DRSC40302 for Nup93-2; DRSC06827/DRSC26470 for Nup50. Sequences can be found on the DRSC website (flyrnai.org). When two amplicons are indicated, we combined equal amounts of both dsRNAs for better efficiency of protein depletion. The second set of amplicons for Nup153, mentioned in Supplementary Fig. 3b, was: BKN45147/DRSC32511.

RNAi depletion

For most experiments dsRNAs were transfected with DOTAP (Roche) following manufacturer's instructions. In Supplementary Fig. 2g, RNAi depletion was executed using a soaking method previously described[74]. Briefly, 15 μg/ml of dsRNA were added to 200 ml of $2.5*10^6$ cells/ml in medium lacking FBS; next cells were incubated for 30 min at room temperature with mild shaking before re-adding FBS. dsRNA derived from the *brown* (*bw*) gene was used as control in all experiments. Incubation times and dsRNA amounts were optimized to maximize depletion efficiency while avoiding toxicity and cell cycle effects. Unless otherwise indicated, cells were treated with dsRNAs for 5 days; Lamin and SUMO were depleted for 4 days. We note that RNAi depletion of nuclear pore components or INMPs does not affect the mCh-HP1a signal or the formation of Nse2 foci (GFP-Nse2 signals after IR), indicating that the heterochromatin domain and early DSB response are intact in these RNAi conditions. Additionally, all kinetics resulting from RNAi depletion must be compared to cells treated with control dsRNAs, since the γH2Av peak shifts from 10 min after IR in non-RNAi experiments (Fig. 1a,c) to 30 min after IR in RNAi controls[15] (*e.g.*, Fig. 2a).

Fluorescence in Situ Hybridization (FISH), Immunofluorescence (IF), TUNEL and imaging of fixed samples

The FISH/IF protocol used in Fig. 5g was previously described[75,76]. Chromosome preparation and FISH protocols used in Fig. 6e were previously described[77]. AACAC and 359bp probes for Fig. 6e were designed as previously described[77] and were purchased from Integrated DNA Technologies. Probe sequences are: 5′-6-FAM-$(AACAC)_7$ and 5′-Cy5-TTTTCCAAATTTCGGTCATCAAATAATCAT, respectively. IF without Triton extraction was used for most experiments as previously described[76]. IF staining of Dgrn, dRad60 and Koi was preceded by a triton extraction step: cells were first settled on polylysine-coated slides, and rinsed twice with CSK Buffer (10 mM PIPES pH7, 100 mM NaCl, 300 mM sucrose, 3 mM $MgCl_2$), then incubated for 5 min with CSK buffer plus 0.5 % Triton X-100. Next, cells were rinsed once in CSK buffer and once in PBS before fixation. The TUNEL Assay was performed as previously described[78]. Imaging and image processing for fixed cells was described previously[15,76,78], and similar approaches were used for imaging chromosome preparations.

Quantitation of Repair Foci in Fixed Samples

In IF experiments, classification of foci inside or outside the DAPI-bright region was done as previously described[15]. Classification of foci inside and outside the heterochromatin

domain in Fig. 6b and Supplementary Figs 6b,c was done by analyzing the position of foci relative to the H3K9me2 staining in each of the Z-stacks. Foci associated with the heterochromatin domain were either inside the H3K9me2 domain, at the periphery of the domain, or at the tips of H3K9me2 protrusions (these categories are similar to those defined previously for the HP1a domain[15], and used in Fig. 1a). Classification of foci at the nuclear periphery was done by analyzing the position of foci relative to a nuclear periphery marker (Lamin, Koi, Nup107 or Nup153). Only the middle Z-stack of each nucleus was used for these quantitations, corresponding to the Z-stack where the nuclear periphery signal is more distinct.

Cell Imaging and Processing in Time-Lapse Experiments

Time-lapse experiments and quantification in Fig. 1a were performed as previously described[15]. For MSD analyses in Fig. 5f, and focus intensity analyses in Fig. 6a, cells were imaged with 40-sec time intervals for 60 min starting from 3–5 min after IR. 10 Z-stacks at 0.8 μm distance were imaged for 0.005 ms for GFP, and 0.015 ms for mCherry. The Coolsnap HQ2 camera was set at 2×2 binning for maximizing the intensity of the light collected and minimizing light exposure. All movies were corrected to compensate for modest photobleaching effects using softWorks (Applied Precision/GE Healthcare). For each nucleus, four stationary and spatially distant foci were tracked with Imaris (Bitplane) and the “correct drift” function of Imaris was applied to these tracks for registering the nucleus. Foci were tracked in 3D using a semiautomated method and manually corrected to ensure optimal connections between timepoints. For Fig. 5f, 1.7 Gy were used rather than 5 Gy, thus reducing the average number of Mu2 foci/nucleus and the frequencies of ambiguous tracks. Focus positional data were extracted in Excel and analyzed in Matlab (MathWorks) using a customized script to derive MSD values. MSDs were calculated as described in[4]. For Fig. 6a, focus intensity data were extracted with Imaris and analyzed in Excel. We identified the time-intervals associated with the movement of each focus in the different zones defined in Fig. 6a, and focus intensity values were normalized to the initial intensity in each zone.

Filament Assay

The filament assay was performed as previously described[15]. Briefly, 250 μl of 8×10^6 cells/ml were spun down after prolonged RNAi depletions (6.5 days), gently resuspended in 100 μl of media, transferred to a polylysine-coated slide, allowed to settle for 12–15 min, and fixed for IF.

IR-sensitivity Assay

To determine cell sensitivity to IR we adapted the Multicolor Competition Assay described in[79] to *Drosophila* cells. Briefly, to determine the sensitivity of cells depleted for a protein of interest relative to control RNAi, cells expressing GFP were treated with control dsRNA, and cells expressing mCherry were treated with dsRNA for the protein of interest (day 0). On day 3, a second round of RNAi was started on the same cultures. On day 4, cells were spun down and washed twice in medium to remove RNAs, combined at 1:1 ratio, and irradiated with 2.5, 5, 7.5, or 10 Gy. On day 7 cells were imaged and quantified. To

determine the sensitivity of control cells we used a similar procedure, with the exception that both GFP- and mCherry- expressing cells were treated with dsRNA for a control protein on day 0. On day 4, mCherry-expressing cells were irradiated and then combined at 1:1 ratio with non-irradiated GFP-expressing cells.

Micronucleus Assay

For detecting micronuclei (Fig. 6d and Supplementary Fig. 6e) dsRNAs were added on day 0, 3, and 7. Cells were irradiated with 10 Gy on day 4, fixed on day 11, and processed for IF analysis. Micronuclei were detected as DAPI-positive signals outside the nuclear periphery.

Apoptosis Assay

For detecting apoptotic cells, dsRNAs were added on day 0, 3, and 7. Cells were irradiated on day 4, fixed on day 11, and processed for IF with antibodies recognizing the active form of Caspase3 (Caspase3/Asp175).

Antibodies

Antibodies used were: anti-Rad51 (1:1000, gift from J. Kadonaga); anti-Lamin/Dm0 (1:500, Developmental Studies Hybridoma Bank, ADL101); anti-Actin (1:1000, Abcam, ab8224); anti-HA (1:1000, Abcam, ab9134 for Western blot; 1:1000, Covance, 16B12 for IF); anti-FLAG (1:1000, Sigma, F1804); anti-Koi (1:1000, gift from J. Fischer and M. Welte); anti-Nup153 (1:200, SDI, Karpen Lab); anti-dPIAS (1:100, Karpen lab); anti-γH2Av (1:1000, Rockland, 600-401-914; 1:100 Developmental Studies Hybridoma Bank, UNC93-5.2.1); anti-GFP (1:1000, Invitrogen, AP11122 for Western blot; 1:1000 Aveles Lab, GFP-1020 for IF; Rockland, 600-101-215 for Ip); anti-Nup107 (1:2000, gift from V. Doye); anti-H3K9me2 (1:500, Upstate, 07-442; 1:750, Wako Chemicals, MABI0307, 302-32369); anti-H3K9me3 (1:500, Active Motif, 39161); anti-SUMO (1:500, SDI, Karpen Lab); anti-Mtor (1:50, SDI, Karpen Lab); anti-FG porins[80] (1:100, Covance, MAb414, MMS-120R); anti-cleaved Caspase3/Asp175 (1:500, Cell Signaling, 5A1E, #9664). Secondary antibodies for IF were from Life Technologies and Jackson Immunoresearch. Those used for western blot were from Pierce and Santa Cruz Biotech.

Statistical Analyses

Unless otherwise indicated, p values were calculated using the Kruskal-Wallis test with multiple-comparison Dunnet's post test. Analyses were done with Prism (Graphpad).

qPCR

Total RNA was isolated from 3–5 × 10^6 cells by Trizol extraction. RNA was used to generate single-stranded cDNA using random priming and Superscript Reverse Transcriptase III (Invitrogen). Specific transcripts were quantified using intron-spanning primers with iQ SYBR Green Supermix (Bio-Rad) and MyiQ Single Color, Real-Time PCR Detection System (Bio-Rad), according to manufacturer's instruction. Changes in transcript levels were normalized to Act5C mRNA. Each qPCR was repeated at least three times, and graphs show the average level of depletion relative to control RNAi. Primer sequences were: TCAGTCGGTTTATTCCAGTC and CAGCAACTTCTTCGTCACACA for Atc5C;

CAGCGCCAATAGCAGTTAATCC and GCACGGTCTGAAGAAATATGGC for dPIAS; GAAGTTGCAGCCCGTTCCAAAG and GGTGCTGCCGCAATTTATAAATCTGG for dRad60; TCACCCAAATGGGCACCAAT and GTCACCGGATCAATCGGCT for Nup93; GGAGGAGGAAAAAGAAGAGGATACG and GGAGTATATAGCGTCATCCTCC for Nup50; ACATCCAAACTGCAAGCCAAC and ACGGTTTCTGGTCTGAACATTTT for Nup160; GGACGCCGTACAAGCATTTG and GATTGCGGCTCTTCTCGCT for Nup205; GCTTGTGGCACAATGATTCGC and CGTTCAATTCGAATCACGGTGCG for Spag4.

Western blotting

1–3 × 10^6 cells were harvested, washed once in PBS and lysed for 15–20 min on ice with lysis buffer A (50 mM Tris, pH 7.8, 1% NP-40, 150 mM NaCl) containing protease inhibitors (Complete, Roche), 2-MercaptoEtOH, and 1 mM PMSF. Benzonase was added to each sample. The soluble lysate was recovered by centrifugation (10 min, 4°C) and resuspended in loading buffer (Laemmli). Samples were denatured by 5 min incubation at 95°C before running them on a TGX 4–12% or 10% gel (Biorad) and transferred onto nitrocellulose membrane for hybridization with specific antibodies.

Immunoprecipitation (Ip)

For dRad60 Ip in Fig. 2c, 3.6 × 10^8 cells expressing FHA-dRad60 and GFP-Dgrn were pelleted and snap-frozen before and after IR. Pellets were incubated in lysis buffer B (50 mM Tris, 150 mM NaCl, 2 mM EDTA, 10% glycerol, 0.2% Nonidet P-40, protease inhibitors (Complete, Roche), 1 mM PMSF, and 25 mM NEM) for 30 min at 4°C. Lysates were pelleted at 4°C, and the supernatant was incubated with FLAG-M2 agarose beads (Sigma) or beads without antibodies as a control, for 5 h at 4°C. Beads were washed 5x with lysis buffer B and heated in loading buffer for 3 min at 95°C for SDS-PAGE. dRad60 Ip in Fig. 2d (Top) was performed as described for Fig. 2c, except that 3 × 10^8 cells expressing FHA-dRad60 (or Kc cells, as a control) were used, and Ip was performed with FLAG-M2 agarose beads for both FHA-dRad60 expressing cells and control cells.

For Dgrn Ip (Fig. 2d, bottom, and Supplementary Fig. 2g), 3.4 × 10^8 cells expressing GFP-Dgrn (or Kc cells, as a control) were pelleted and snap-frozen before and after IR. Pellets were incubated in lysis buffer C (50 mM Hepes, 10 mM KCl, 2 mM $MgCl_2$, 20% Glycerol, 1 mM PMSF, 20 mM NaF, 20 mM Glycerol-2-phosphate, 1 mM benzamidine, 0.5% NP-40, 25 mM NEM, 150 mM NaOAc, 250 mM NaCl, and protease inhibitors (Complete, Roche)), and digested with benzonase at 4°C for 30 min. After isolating soluble lysates by centrifugation, pellets were resuspended in buffer C, extracted with 300 mM sodium acetate for 1 h at 4°C, and the supernatant was pooled with the soluble lysate. Samples were incubated for 3 h at 4°C with Protein G-coupled sepharose beads and 5 μl of goat anti-GFP antibody. Beads were washed 5x with wash buffer C (50 mM Hepes, 10 mM KCl, 2 mM $MgCl_2$, 20% Glycerol, 0.5% NP-40, 350 mM NaCl, 150 mM NaOAc, and 25 mM NEM), and then heated in loading buffer for 3 min at 95°C for SDS-PAGE.

Fly stocks and crosses

All fly stocks were raised at 25°C. We received *dPIAS*^{1} and *dPIAS*^{2}, *drad60*^{51} (*CG4449*^{MI12051}), *nup107*^{E8}, and *smc5*^{GS14577} from the Bloomington *Drosophila* stock

center (BDSC). dgrn^{DK} was from A. Orian and S. Parkhurst[37]. We generated *smc5* mutant alleles by mobilization of the *P{GSV6}* element in the *smc5*^{GS14577} genotype. Imprecise excisions generated the *smc5*^{7} and *smc5*^{19} alleles. *smc5*^{19} sequencing revealed a frameshift in the second exon, leading to an early stop codon. We did not obtain PCR amplifications and sequence for the *smc5*^{7} allele, suggesting a large deletion. The absence of Smc5 protein in *smc5*^{7} *and smc5*^{19} mutants was confirmed by Western blotting (Supplementary Fig. 6f). The perfect excision in the *Smc5*^{17} *allele* was confirmed by Western blotting (Supplementary Fig. 6g) and sequencing, and used as a control in addition to the standard control *y*^{1}*; ry*^{506} (*yry).* Genotypes used in Fig. 6e and Supplementary Fig. 6g were: *smc5*$^{7/19}$ *(smc5), dPIAS*$^{1/2}$ *(dPIAS)*[26], *drad60*$^{51/51}$*(drad60), dgrn*$^{DK/DK}$ *(dgrn), nup107*^{E8}*/CyO (nup107)*[81] *and the Wt controls yry and Smc5*$^{17/17}$. All homozygous and trans-heterozygous mutants, except for *dRad60*, were generated by crossing heterozygous parents maintained as balanced stocks. *dRad60* mutants were generated from homozygous parents.

Supplementary Material

Refer to Web version on PubMed Central for supplementary material.

Acknowledgments

This work was supported by the USC Gold Family Fellowship and the USC Research Enhancement Fellowship to T.R.; the USC Provost Fellowship to B.S.; R21ES021541, The Rose Hills Foundation, and R01GM117376 to I.C.; R01GM086613 to G.H.K. We would like to thank S. Keagy, M. Michael, J. Haber and O. Aparicio for insightful comments on the manuscript, and S. Gasser for sharing results before publication. We are grateful to V. Doye, J. Kadonaga, J. Fischer, M. Welte, A. Orian, S. Parkhurst, A. Ashworth and the O. Aparicio lab for sharing reagents and the Chiolo and Karpen labs for helpful discussions. We thank C. Ferraro and N. Brisson for their help with Lamin and SUMO RNAi studies, and J. Swenson for his initial dPIAS RNAi studies. We also thank M. Bonner for generating the mCh-LaminC construct, D. Das, E. Lin and C. Ren for cloning and RNAi reagents, A. Kim, S. Wijekularatne and N. Saxena for cloning and Smc5 mutant characterization. Fly stocks from BDSC (NIH P40OD018537) and RNAi libraries from DRSC (NIH R01GM067761) were used for this study.

References

1. Nagai S, et al. Functional targeting of DNA damage to a nuclear pore-associated SUMO-dependent ubiquitin ligase. Science. 2008; 322:597–602. [PubMed: 18948542]
2. Oza P, Jaspersen SL, Miele A, Dekker J, Peterson CL. Mechanisms that regulate localization of a DNA double-strand break to the nuclear periphery. Genes Dev. 2009; 23:912–927. [PubMed: 19390086]
3. Dion V, Kalck V, Horigome C, Towbin BD, Gasser SM. Increased mobility of double-strand breaks requires Mec1, Rad9 and the homologous recombination machinery. Nat Cell Biol. 2012; 14:502–509. [PubMed: 22484486]
4. Miné-Hattab J, Rothstein R. Increased chromosome mobility facilitates homology search during recombination. Nat Cell Biol. 2012; 14:510–517. [PubMed: 22484485]
5. Horigome C, et al. SWR1 and INO80 Chromatin Remodelers Contribute to DNA Double-Strand Break Perinuclear Anchorage Site Choice. Mol Cell. 2014; 55:626–639. [PubMed: 25066231]
6. Kalocsay M, Hiller NJ, Jentsch S. Chromosome-wide Rad51 spreading and SUMO-H2A.Z-dependent chromosome fixation in response to a persistent DNA double-strand break. Mol Cell. 2009; 33:335–343. [PubMed: 19217407]
7. Su XA, Dion V, Gasser SM, Freudenreich CH. Regulation of recombination at yeast nuclear pores controls repair and triplet repeat stability. Genes Dev. 2015; 29:1006–1017. [PubMed: 25940904]
8. Ho JW, et al. Comparative analysis of metazoan chromatin organization. Nature. 2014; 512:449–452. [PubMed: 25164756]

9. Hoskins RA, et al. Sequence Finishing and Mapping of Drosophila melanogaster Heterochromatin. Science. 2007; 316:1625–1628. [PubMed: 17569867]
10. Smith CD, Shu S, Mungall CJ, Karpen GH. The Release 5.1 annotation of Drosophila melanogaster heterochromatin. Science. 2007; 316:1586–1591. [PubMed: 17569856]
11. Hoskins RA, et al. The Release 6 reference sequence of the Drosophila melanogaster genome. Genome Res. 2015; 25:445–458. [PubMed: 25589440]
12. Riddle NC, et al. Plasticity in patterns of histone modifications and chromosomal proteins in Drosophila heterochromatin. Genome Res. 2011; 21:147–163. [PubMed: 21177972]
13. Peng JC, Karpen GH. Epigenetic regulation of heterochromatic DNA stability. Curr Opin Genet Dev. 2008; 18:204–211. [PubMed: 18372168]
14. Chiolo I, Tang J, Georgescu W, Costes SV. Nuclear dynamics of radiation-induced foci in euchromatin and heterochromatin. Mutat Res. 2013; 750:56–66. [PubMed: 23958412]
15. Chiolo I, et al. Double-strand breaks in heterochromatin move outside of a dynamic HP1a domain to complete recombinational repair. Cell. 2011; 144:732–744. [PubMed: 21353298]
16. Dronamraju R, Mason JM. MU2 and HP1a regulate the recognition of double strand breaks in Drosophila melanogaster. PLoS ONE. 2011; 6:e25439. [PubMed: 21966530]
17. Jakob B, et al. DNA double-strand breaks in heterochromatin elicit fast repair protein recruitment, histone H2AX phosphorylation and relocation to euchromatin. Nucleic Acids Res. 2011; 39:6489–6499. [PubMed: 21511815]
18. Torres-Rosell J, et al. The Smc5-Smc6 complex and SUMO modification of Rad52 regulates recombinational repair at the ribosomal gene locus. Nat Cell Biol. 2007; 9:923–931. [PubMed: 17643116]
19. Andrews EA, et al. Nse2, a component of the Smc5-6 complex, is a SUMO ligase required for the response to DNA damage. Mol Cell Biol. 2005; 25:185–196. [PubMed: 15601841]
20. Potts PR, Yu H. Human MMS21/NSE2 is a SUMO ligase required for DNA repair. Mol Cell Biol. 2005; 25:7021–7032. [PubMed: 16055714]
21. Zhao X, Blobel G. A SUMO ligase is part of a nuclear multiprotein complex that affects DNA repair and chromosomal organization. Proc Natl Acad Sci U S A. 2005; 102:4777–4782. [PubMed: 15738391]
22. Reindle A, et al. Multiple domains in Siz SUMO ligases contribute to substrate selectivity. J Cell Sci. 2006; 119:4749–4757. [PubMed: 17077124]
23. Cremona CA, et al. Extensive DNA damage-induced sumoylation contributes to replication and repair and acts in addition to the mec1 checkpoint. Mol Cell. 2012; 45:422–432. [PubMed: 22285753]
24. Psakhye I, Jentsch S. Protein Group Modification and Synergy in the SUMO Pathway as Exemplified in DNA Repair. Cell. 2012:1–14.
25. Albuquerque CP, et al. Distinct SUMO ligases cooperate with Esc2 and Slx5 to suppress duplication-mediated genome rearrangements. PLoS Genet. 2013; 9:e1003670. [PubMed: 23935535]
26. Hari KL, Cook KR, Karpen GH. The DrosophilaSu(var)2-10Locus Encodes A Member of the PIAS Protein Family and Regulates Chromosome Structure and Function. Genes and Development. 2001; 15:1334–1348. [PubMed: 11390354]
27. Jackson SP, Durocher D. Regulation of DNA damage responses by ubiquitin and SUMO. Molecular cell. 2013; 49:795–807. [PubMed: 23416108]
28. Nagai S, Davoodi N, Gasser SM. Nuclear organization in genome stability: SUMO connections. Cell Res. 2011; 21:474–485. [PubMed: 21321608]
29. Burgess RC, Rahman S, Lisby M, Rothstein R, Zhao X. The Slx5-Slx8 complex affects sumoylation of DNA repair proteins and negatively regulates recombination. Mol Cell Biol. 2007; 27:6153–6162. [PubMed: 17591698]
30. Galanty Y, Belotserkovskaya R, Coates J, Jackson SP. RNF4, a SUMO-targeted ubiquitin E3 ligase, promotes DNA double-strand break repair. Genes Dev. 2012; 26:1179–1195. [PubMed: 22661229]

31. Yin Y, et al. SUMO-targeted ubiquitin E3 ligase RNF4 is required for the response of human cells to DNA damage. Genes & development. 2012; 26:1196–1208. [PubMed: 22661230]
32. Prudden J, et al. SUMO-targeted ubiquitin ligases in genome stability. EMBO J. 2007; 26:4089–4101. [PubMed: 17762865]
33. Heideker J, Prudden J, Perry JJP, Tainer JA, Boddy MN. SUMO-targeted ubiquitin ligase, Rad60, and Nse2 SUMO ligase suppress spontaneous Top1-mediated DNA damage and genome instability. PLoS Genet. 2011; 7:e1001320. [PubMed: 21408210]
34. Novatchkova M, Bachmair A, Eisenhaber B, Eisenhaber F. Proteins with two SUMO-like domains in chromatin-associated complexes: the RENi (Rad60-Esc2-NIP45) family. BMC Bioinformatics. 2005; 6:22. [PubMed: 15698469]
35. Sun H, Leverson JD, Hunter T. Conserved function of RNF4 family proteins in eukaryotes: targeting a ubiquitin ligase to SUMOylated proteins. EMBO J. 2007; 26:4102–4112. [PubMed: 17762864]
36. Boddy MN, et al. Replication checkpoint kinase Cds1 regulates recombinational repair protein Rad60. Mol Cell Biol. 2003; 23:5939–5946. [PubMed: 12897162]
37. Barry KC, et al. The Drosophila STUbL protein Degringolade limits HES functions during embryogenesis. Development. 2011; 138:1759–1769. [PubMed: 21486924]
38. Prudden J, Perry JJP, Arvai AS, Tainer JA, Boddy MN. Molecular mimicry of SUMO promotes DNA repair. Nat Struct Mol Biol. 2009; 16:509–516. [PubMed: 19363481]
39. Sekiyama N, et al. Structural basis for regulation of poly-SUMO chain by a SUMO-like domain of Nip45. Proteins. 2010; 78:1491–1502. [PubMed: 20077568]
40. Miyabe I, Morishita T, Hishida T, Yonei S, Shinagawa H. Rhp51-dependent recombination intermediates that do not generate checkpoint signal are accumulated in Schizosaccharomyces pombe rad60 and smc5/6 mutants after release from replication arrest. Mol Cell Biol. 2006; 26:343–353. [PubMed: 16354704]
41. Zhang C, Roberts TM, Yang J, Desai R, Brown GW. Suppression of genomic instability by SLX5 and SLX8 in Saccharomyces cerevisiae. DNA repair. 2006; 5:336–346. [PubMed: 16325482]
42. Sollier J, et al. The Saccharomyces cerevisiae Esc2 and Smc5-6 proteins promote sister chromatid junction-mediated intra-S repair. Mol Biol Cell. 2009; 20:1671–1682. [PubMed: 19158389]
43. Sabri N, et al. Distinct functions of the Drosophila Nup153 and Nup214 FG domains in nuclear protein transport. J Cell Biol. 2007; 178:557–565. [PubMed: 17682050]
44. Razafsky D, Hodzic D. Bringing KASH under the SUN: the many faces of nucleo-cytoskeletal connections. J Cell Biol. 2009; 186:461–472. [PubMed: 19687252]
45. Lenz-Bohme B, et al. Insertional mutation of the Drosophila nuclear lamin Dm0 gene results in defective nuclear envelopes, clustering of nuclear pore complexes, and accumulation of annulate lamellae. J Cell Biol. 1997; 137:1001–1016. [PubMed: 9166402]
46. Capelson M, et al. Chromatin-bound nuclear pore components regulate gene expression in higher eukaryotes. Cell. 2010; 140:372–383. [PubMed: 20144761]
47. Kalverda B, Pickersgill H, Shloma VV, Fornerod M. Nucleoporins directly stimulate expression of developmental and cell-cycle genes inside the nucleoplasm. Cell. 2010; 140:360–371. [PubMed: 20144760]
48. Vaquerizas JM, et al. Nuclear pore proteins nup153 and megator define transcriptionally active regions in the Drosophila genome. PLoS Genet. 2010; 6:e1000846. [PubMed: 20174442]
49. Barton LJ, Soshnev AA, Geyer PK. Networking in the nucleus: a spotlight on LEM-domain proteins. Curr Opin Cell Biol. 2015; 34:1–8. [PubMed: 25863918]
50. Brough R, et al. Functional analysis of Drosophila melanogaster BRCA2 in DNA repair. DNA Repair (Amst). 2008; 7:10–19. [PubMed: 17822964]
51. Liu J, Doty T, Gibson B, Heyer WD. Human BRCA2 protein promotes RAD51 filament formation on RPA-covered single-stranded DNA. Nat Struct Mol Biol. 2010; 17:1260–1262. [PubMed: 20729859]
52. Dronamraju R, Mason JM. Recognition of double strand breaks by a mutator protein (MU2) in Drosophila melanogaster. PLoS Genet. 2009; 5:e1000473. [PubMed: 19424425]

53. Zou L, Elledge SJ. Sensing DNA damage through ATRIP recognition of RPA-ssDNA complexes. Science. 2003; 300:1542–1548. [PubMed: 12791985]
54. Zhu Z, Chung WH, Shim EY, Lee SE, Ira G. Sgs1 helicase and two nucleases Dna2 and Exo1 resect DNA double-strand break ends. Cell. 2008; 134:981–994. [PubMed: 18805091]
55. Cortez D, Guntuku S, Qin J, Elledge SJ. ATR and ATRIP: partners in checkpoint signaling. Science. 2001; 294:1713–1716. [PubMed: 11721054]
56. Pellicioli A, Lee SE, Lucca C, Foiani M, Haber JE. Regulation of Saccharomyces Rad53 checkpoint kinase during adaptation from DNA damage-induced G2/M arrest. Mol Cell. 2001; 7:293–300. [PubMed: 11239458]
57. Hatch EM, Fischer AH, Deerinck TJ, Hetzer MW. Catastrophic nuclear envelope collapse in cancer cell micronuclei. Cell. 2013; 154:47–60. [PubMed: 23827674]
58. Fenech M, et al. Molecular mechanisms of micronucleus, nucleoplasmic bridge and nuclear bud formation in mammalian and human cells. Mutagenesis. 2011; 26:125–132. [PubMed: 21164193]
59. Xie Y, et al. The yeast Hex3.Slx8 heterodimer is a ubiquitin ligase stimulated by substrate sumoylation. J Biol Chem. 2007; 282:34176–34184. [PubMed: 17848550]
60. Kosoy A, Calonge TM, Outwin EA, O'Connell MJ. Fission yeast Rnf4 homologs are required for DNA repair. The Journal of biological chemistry. 2007; 282:20388–20394. [PubMed: 17502373]
61. Uzunova K, et al. Ubiquitin-dependent proteolytic control of SUMO conjugates. The Journal of biological chemistry. 2007; 282:34167–34175. [PubMed: 17728242]
62. Guzzo CM, et al. RNF4-dependent hybrid SUMO-ubiquitin chains are signals for RAP80 and thereby mediate the recruitment of BRCA1 to sites of DNA damage. Sci Signal. 2012; 5:ra88. [PubMed: 23211528]
63. Groocock LM, et al. RNF4 interacts with both SUMO and nucleosomes to promote the DNA damage response. EMBO Rep. 2014; 15:601–608. [PubMed: 24714598]
64. Eladad S, et al. Intra-nuclear trafficking of the BLM helicase to DNA damage-induced foci is regulated by SUMO modification. Human molecular genetics. 2005; 14:1351–1365. [PubMed: 15829507]
65. Branzei D, et al. Ubc9- and mms21-mediated sumoylation counteracts recombinogenic events at damaged replication forks. Cell. 2006; 127:509–522. [PubMed: 17081974]
66. Goodarzi AA, Kurka T, Jeggo PA. KAP-1 phosphorylation regulates CHD3 nucleosome remodeling during the DNA double-strand break response. Nat Struct Mol Biol. 2011; 18:831–839. [PubMed: 21642969]
67. Kuo CY, et al. An Arginine-rich Motif of Ring Finger Protein 4 (RNF4) Oversees the Recruitment and Degradation of the Phosphorylated and SUMOylated Kruppel-associated Box Domain-associated Protein 1 (KAP1)/TRIM28 Protein during Genotoxic Stress. The Journal of biological chemistry. 2014; 289:20757–20772. [PubMed: 24907272]
68. Khadaroo B, et al. The DNA damage response at eroded telomeres and tethering to the nuclear pore complex. Nat Cell Biol. 2009; 11:980–987. [PubMed: 19597487]
69. Staeva-Vieira E, Yoo S, Lehmann R. An essential role of DmRad51/SpnA in DNA repair and meiotic checkpoint control. Embo J. 2003; 22:5863–5874. [PubMed: 14592983]
70. Joyce EF, Williams BR, Xie T, Wu CT. Identification of genes that promote or antagonize somatic homolog pairing using a high-throughput FISH-based screen. PLoS Genet. 2012; 8:e1002667. [PubMed: 22589731]
71. Cherbas L, Gong L. Cell lines. Methods. 2014; 68:74–81. [PubMed: 24434506]
72. Costes SV, Chiolo I, Pluth JM, Barcellos-Hoff MH, Jakob B. Spatiotemporal characterization of ionizing radiation induced DNA damage foci and their relation to chromatin organization. Mutation Research. 2010; 704:78–87. [PubMed: 20060491]
73. Cheeseman IM, Desai A. A combined approach for the localization and tandem affinity purification of protein complexes from metazoans. Sci STKE. 2005:pl1. [PubMed: 15644491]
74. Zhou R, Mohr S, Hannon GJ, Perrimon N. Inducing RNAi in Drosophila cells by soaking with dsRNA. Cold Spring Harb Protoc. 2014
75. Dernburg AF, et al. Perturbation of nuclear architecture by long-distance chromosome interactions. Cell. 1996; 85:745–759. [PubMed: 8646782]

76. Peng JC, Karpen GH. H3K9 methylation and RNA interference regulate nucleolar organization and repeated DNA stability. Nat Cell Biol. 2007; 9:25–35. [PubMed: 17159999]

77. Larracuente AM, Ferree PM. Simple method for fluorescence DNA in situ hybridization to squashed chromosomes. Journal of visualized experiments : JoVE. 2015:52288. [PubMed: 25591075]

78. Peng JC, Karpen GH. Heterochromatic genome stability requires regulators of histone H3 K9 methylation. PLoS Genet. 2009; 5:e1000435. [PubMed: 19325889]

79. Smogorzewska A, et al. Identification of the FANCI protein, a monoubiquitinated FANCD2 paralog required for DNA repair. Cell. 2007; 129:289–301. [PubMed: 17412408]

80. Davis LI, Blobel G. Nuclear pore complex contains a family of glycoproteins that includes p62: glycosylation through a previously unidentified cellular pathway. Proceedings of the National Academy of Sciences of the United States of America. 1987; 84:7552–7556. [PubMed: 3313397]

81. Katsani KR, Karess RE, Dostatni N, Doye V. In vivo dynamics of Drosophila nuclear envelope components. Mol Biol Cell. 2008; 19:3652–3666. [PubMed: 18562695]

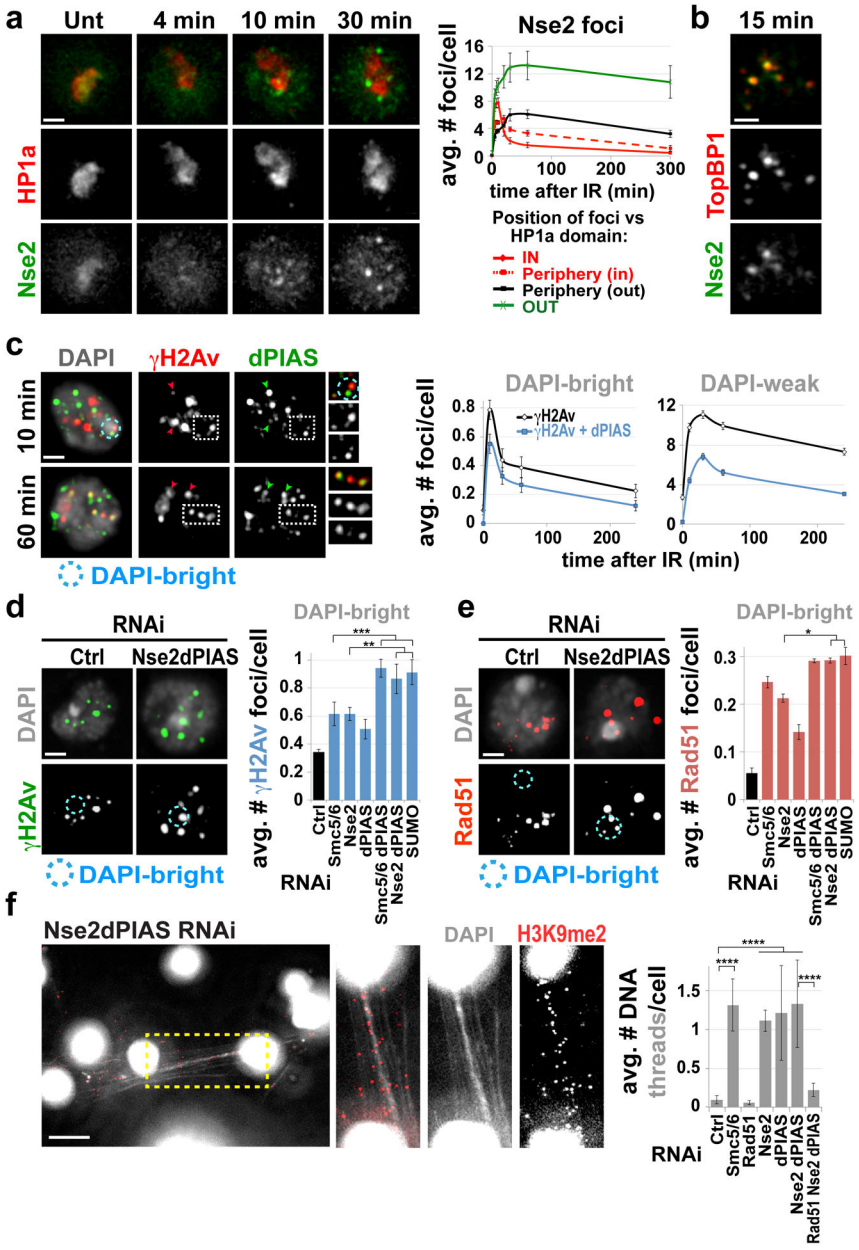

Figure 1. SUMOylation blocks HR progression in heterochromatin and promotes DSB relocalization

(**a**) Live imaging (left) and quantitation (right) show GFP-Nse2 relative to mCh-HP1a (heterochromatin marker[15]) before (Unt, 0) and after IR. Nse2 focus relocalization results in reduction of focus number inside the heterochromatin domain (IN) between 10 and 30 min after IR (error bars: s.e.m, p = 0.0001 for 10 vs. 30 min, two-tailed Mann-Whitney test, n = 9 cells from one experiment), concurrently with focus increase at the periphery of the heterochromatin domain (periphery in/out), and in the euchromatic space (OUT)[15].

(**b**) Live imaging shows GFP-Nse2 and mCh-TopBP1 foci 15 min after IR.

(**c**) Immunofluorescence (IF) (left) and quantitation (right) show the number of γH2Av foci colocalizing with dPIAS foci in DAPI-bright (heterochromatin[15]) and DAPI-weak

(euchromatin[15]) at different timepoints after IR. Arrowheads and zoomed details highlight colocalizations. Error bars: s.e.m., n = 100 cells for each timepoint from one experiment.
(**d**) IF analysis (left) and quantitation (right) of cells fixed 60 min after IR show the number of γH2Av foci in DAPI-bright after RNAi depletions ($p < 0.0001$ for all comparisons vs. Ctrl RNAi; $^{**}p < 0.01$, $^{***}p < 0.001$, one-tailed Mann-Whitney test; $n > 180$ cells). RNAi efficiencies are shown in Supplementary Figs 1e,g–i.
(**e**) As described in (d), except cells were stained for Rad51 ($p < 0.0001$ for all comparisons vs. Ctrl; $^{*}p < 0.05$, one-tailed Mann-Whitney test; $n > 200$ cells).
(f) Filament assay[15] and quantitation (right) of cells stained for DAPI and H3K9me2 show the formation of heterochromatic DNA filaments connecting dividing cells after RNAi depletions ($^{****}p < 0.0001$; $n > 700$ cells). Examples of filaments (left) are shown as zoomed detail of the outlined region. Rad51 RNAi efficiency is shown in Supplementary Fig. 1l.
Ctrl = control. Scale bars = 1 μm (a–e) or 5 μm (f). Images are one Z-stack in (c), maximum intensity projections of the nucleus in (a,b,f), or Z-stacks spanning the DAPI-bright region in (d,e). In (d–f), the error bars represent mean +/− s.d. derived from three independent experiments, whereas the sample size (n) used to determine p values is the total number of cells for each RNAi, pooled across the three experiments. Exact n values are in Supplementary Table 1.

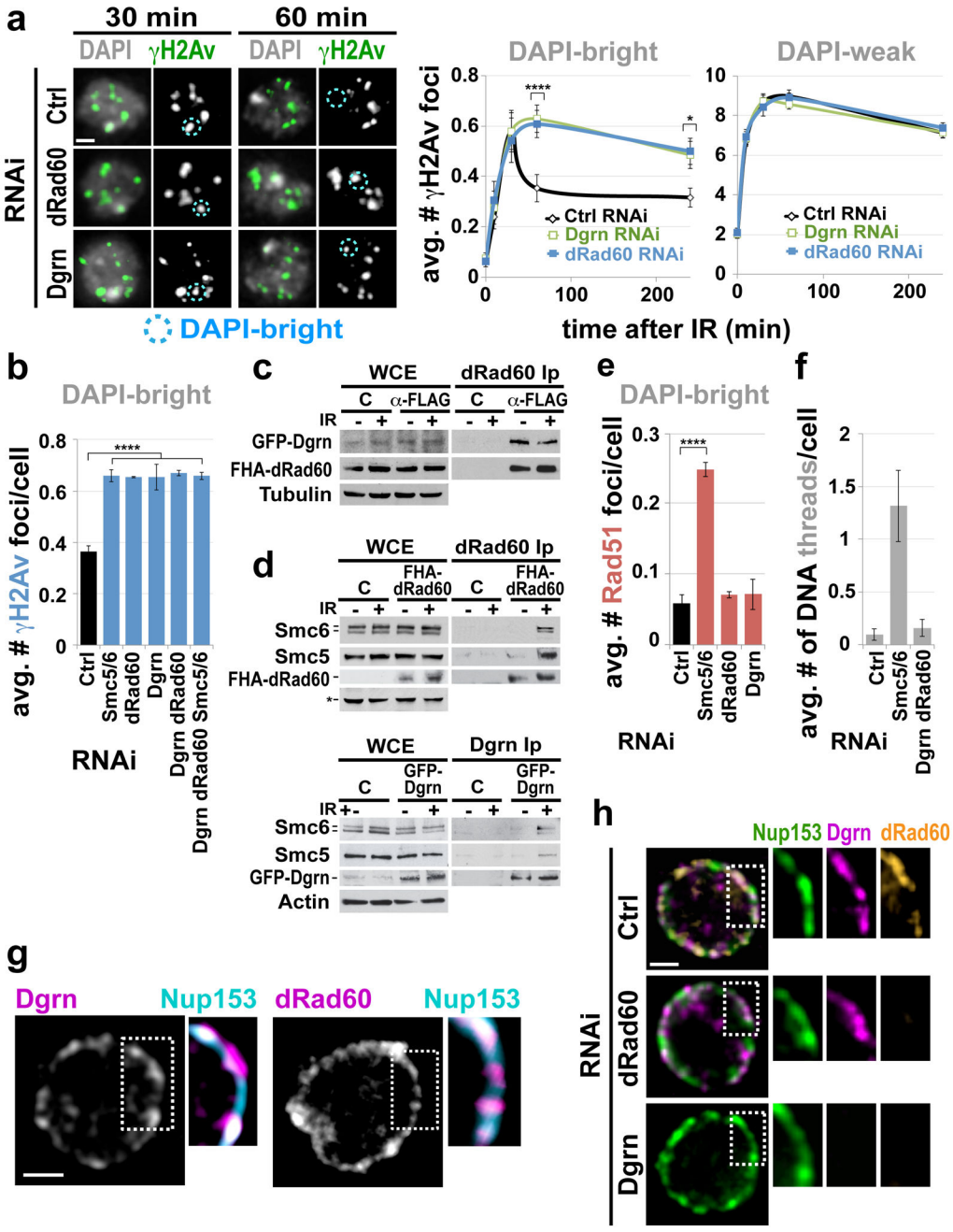

Figure 2. STUbL/RENi proteins work with Smc5/6 to relocalize heterochromatic DSBs

(**a**) IF (left) and quantitation (right) of cells fixed before and after IR show the number of γH2Av foci in DAPI-bright/weak after RNAi depletions (error bars: s.e.m.; ****$p < 0.0001$ and *$p < 0.05$ for dRad60/Dgrn vs. Ctrl RNAi, one-tailed Mann-Whitney test with $n > 140$ cells/timepoint/RNAi condition from one experiment). Note: because of the low number of foci in DAPI-bright, DAPI-weak focus numbers are similar to total foci. See Supplementary Figs 2a,b for RNAi efficiencies.

(**b**) As described in (a) except cells were fixed only 60 min after IR (****$p < 0.0001$, $n > 160$ cells). Epistasis was confirmed at other IR doses (Supplementary Fig. 2d).
(**c**) Immunoprecipitation (Ip) of dRad60 in cells expressing FHA-dRad60 and GFP-Dgrn before (−) and 45 min after (+) IR (20 Gy), and Western analysis with anti-GFP, HA, and tubulin (loading control) antibodies.
(**d**) As described in (c) except dRad60 Ip (top) was done in cells expressing FHA-dRad60, and Dgrn Ip (bottom) in cells expressing GFP-Dgrn; Western analyses were done with anti-HA (top), GFP (bottom), Smc5, Smc6 antibodies. Actin or a nonspecific band (*) is the loading control.
(**e**) As described in (b) except cells were stained for Rad51 (****$p < 0.0001$, $n > 190$ cells).
(f) Quantitations show the number of DNA filaments connecting dividing cells after RNAi depletions and filament assay ($n > 700$ cells). Smc5/Ctrl RNAi samples are from Fig. 1f.
(**g**) IF of cells expressing GFP-Dgrn (left) and FHA-dRad60 (right), and stained for nuclear periphery (Nup153/zoomed detail), and either GFP (left) or HA (right).
(**h**) IF of cells expressing FHA-dRad60 and GFP-Dgrn after RNAi depletions. Effects on dRad60/Dgrn associations with the periphery are shown in zoomed details.
Ctrl/C = control. Scale bars = 1 μm. WCE = whole cell extract. Images are maximum intensity projections of Z-stacks spanning the DAPI-bright region in (a), or middle Z-stacks in (g,h). In (b,e,f), the error bars represent mean +/− s.d. from three independent experiments, whereas the sample size (n) used to determine p values in (b,e) is the total number of cells for each RNAi, pooled across the three experiments. Exact n values are in Supplementary Table 1. Uncropped Western blot scans are in Supplementary Fig. 7.

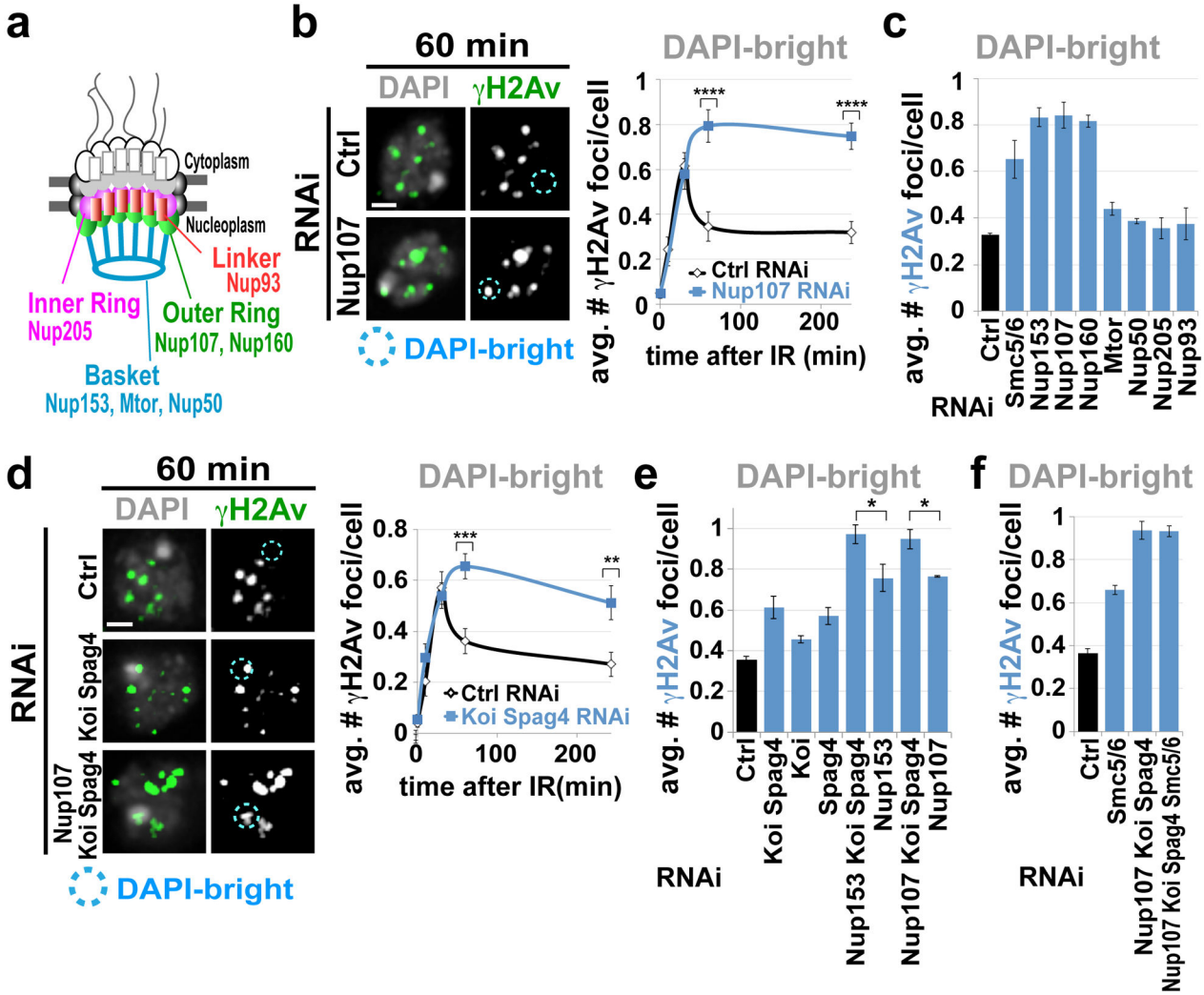

Figure 3. Nuclear pores and INMPs are required for relocalizing heterochromatic DSBs

(**a**) Schematic view of the nuclear pore highlighting the subunits analyzed.

(**b**) IF analysis (left) and quantitation (right) of cells fixed before and at different timepoints after IR show the number of γH2Av foci in DAPI-bright after RNAi depletion of the indicated proteins (error bars: s.e.m., ****p < 0.0001 for Nup107 vs. Ctrl RNAi, two-tailed Mann-Whitney test with n > 130 cells for each timepoint and RNAi condition from one experiment). Nup107 RNAi efficiency is shown in Supplementary Fig. 3a.

(**c**) Quantitation of an experiment performed as described in (b) except analysis was done only at 60 min after IR (p < 0.0001 for Nup153, Nup107, or Nup160 RNAi vs. Ctrl RNAi, with n > 180 cells). RNAi efficiencies and effects on nuclear pore stability are shown in Supplementary Fig. 3a,b.

(**d**) As described in (b) (error bars: s.e.m.; ***p < 0.005 and **p < 0.01 for Koi+Spag4 vs. Ctrl RNAi, two-tailed Mann-Whitney test with n > 80 cells for each timepoint and RNAi condition from one experiment). RNAi efficiencies are shown in Supplementary Fig. 3a.

(**e**) As described in (c) ($p < 0.05$ for Koi RNAi vs. Ctrl RNAi, $p < 0.0001$ for all other RNAi vs. Ctrl RNAi, *$p < 0.05$, two-tailed Mann-Whitney test with $n > 170$ cells).
(**f**) As described in (c). Similar numbers of persistent γH2Av foci are observed in DAPI-bright after Nup107+Koi+Spag4 RNAi, or Nup107+Koi+Spag4+Smc5/6 RNAi, and both are higher than control and Smc5/6 RNAi ($p < 0.0001$, $n > 160$ cells).
Ctrl = control. Scale bars = 1 μm. Images are maximum intensity projections of Z-stacks spanning the DAPI-bright region. In (c,e,f), the error bars represent mean +/− s.d. from three independent experiments, whereas the sample size (n) used to determine p values is the total number of cells for each RNAi, pooled across the three experiments. Exact n values are in Supplementary Table 1.

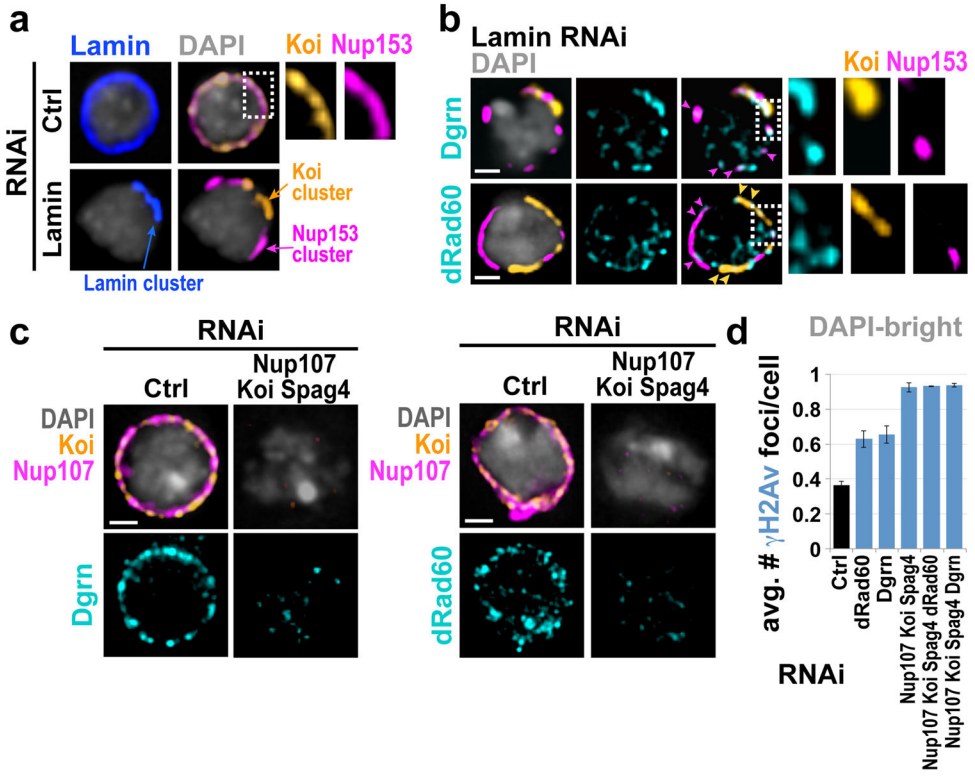

Figure 4. Nuclear pores and INMPs recruit STUbL/RENi to the nuclear periphery and work with STUbL/RENi for DSB relocalization

(**a**) IF analyses of Lamin, Koi and Nup153 show the formation of Koi and Nup153 clusters after Lamin RNAi and not in Ctrl RNAi. RNAi efficiency is shown in Supplementary Fig. 4a.

(**b**) IF analyses of cells expressing FHA-dRad60 and GFP-Dgrn after lamin RNAi, and stained for Nup153, Koi, and GFP (top) or HA (bottom), show colocalizations of Dgrn or dRad60 with Nup153 or Koi clusters (arrows and zoomed details of the outlined regions).

(**c**) IF analyses of cells expressing FHA-dRad60 and GFP-Dgrn and stained for Nup107, Koi, and either GFP (left) or HA (right), show the effects of RNAi depletions on Dgrn/dRad60 association with the nuclear periphery.

(**d**) RNAi depletion of indicated components was performed and cells were fixed 60 min after IR and stained for γH2Av. Quantitation shows that simultaneous RNAi depletion of Nup107+Koi+Spag4 results in the same number of γH2Av foci in DAPI-bright as the depletion of Nup107+Koi+Spag4 plus dRad60 or Dgrn, and all are higher than observed in control RNAi ($p < 0.0001$, $n > 190$ cells). The error bars represent mean +/− s.d. from three independent experiments whereas the sample size used to determine p values is the total number of cells for each RNAi, pooled across the three experiments. Exact n values are in Supplementary Table 1.

Ctrl = control. Scale bars = 1 μm. Images are middle Z-stacks of nuclei.

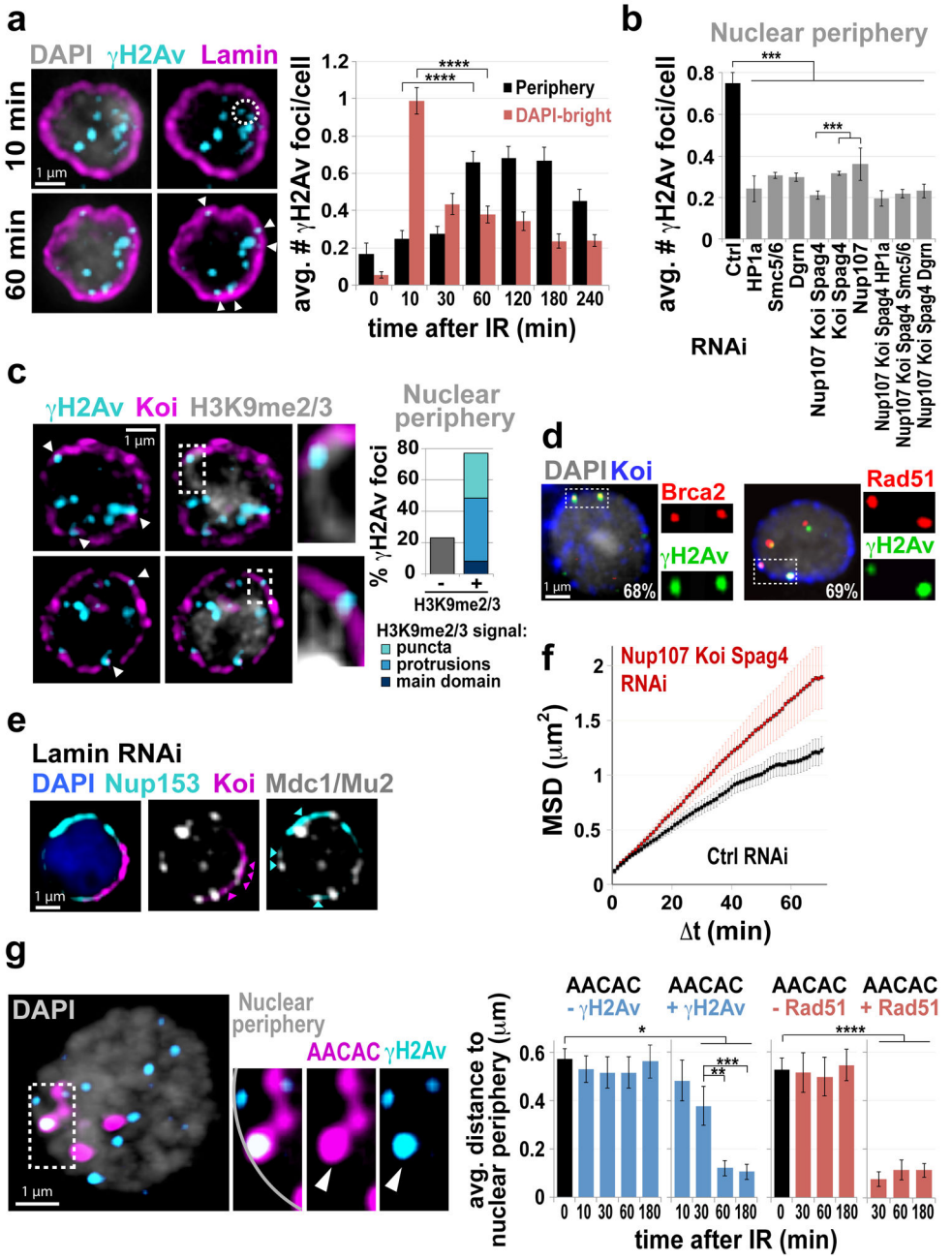

Figure 5. Heterochromatic DSBs relocalize to nuclear periphery

(**a**) IF (left) and quantitation (right) of cells fixed before and after IR, stained for γH2Av/Lamin/DAPI (error bars: s.e.m.; ****p < 0.0001, two-tailed Mann-Whitney test with n > 150 cells/timepoint from one or more experiments). Quantitations of foci at the nuclear periphery (Lamin/arrowheads) or in heterochromatin (DAPI-bright/dashed circle) were done using middle Z-stacks or all Z-stacks, respectively.

(**b**) Quantitation using middle Z-stacks of γH2Av foci colocalizing with Lamin 60 min post IR, after RNAi depletions (***p < 0.005, one-tailed Mann-Whitney test, n > 140 cells/RNAi; error bars: mean +/− s.d. from at least three independent experiments; (n) used to

determine p values is the total number of cells pooled across all experiments). HP1a RNAi efficiency is in Supplementary Fig. 5b.

(**c**) IF (left) of cells fixed 60 min after IR, stained for γH2Av, H3K9me2/3 (heterochromatin) and Koi (nuclear periphery). Quantitation (right) shows the proportions of nuclear periphery-associated γH2Av foci (arrowheads) colocalizing with heterochromatin: main domain, protrusions (zoomed details), or puncta (n = 400 foci, one experiment).

(**d**) IF of cells expressing (left) or not expressing (right) FHA-Brca2, fixed 60 min after IR, stained for Koi/γH2Av plus HA (left) or Rad51 (right). % of periphery-associated γH2Av foci colocalizing with Brca2/Rad51 foci (zoomed details) is indicated.

(**e**) IF for Nup153/Koi/GFP in GFP-Mu2/Mdc1-expressing cells, fixed 60 min post IR after Lamin RNAi, shows foci colocalizing with Nup153/Koi clusters (arrowheads).

(**f**) MSD analysis of GFP-Mu2/Mdc1 foci leaving the mCh-HP1a domain after RNAi depletions (error bars: s.e.m., $p < 0.0001$, Wilcoxon matched-pairs signed rank test, $n > 30$ foci/RNAi from one experiment). Curve plateaus are proportional to the radius of constraint[3,4].

(**g**) Fluorescence in situ hybridization (FISH)/IF of cells fixed before and after IR, stained for AACAC/DAPI plus γH2Av or Rad51. Left: Example of nuclear periphery (DAPI periphery)-associated AACAC signals colocalizing with γH2Av 60 min after IR. Right: Quantitation of the distance to nuclear periphery of AACAC associated (+) or not associated (−) with γH2Av/Rad51 (error bars: s.e.m.; *$p < 0.05$, **$p < 0.02$, ***$p < 0.01$, ****$p < 0.0001$, two tailed Mann-Whitney test with $n > 14$ foci for each timepoint from one experiment).

Ctrl = control. Images are middle Z-stacks of nuclei. Exact n values are in Supplementary Table 1.

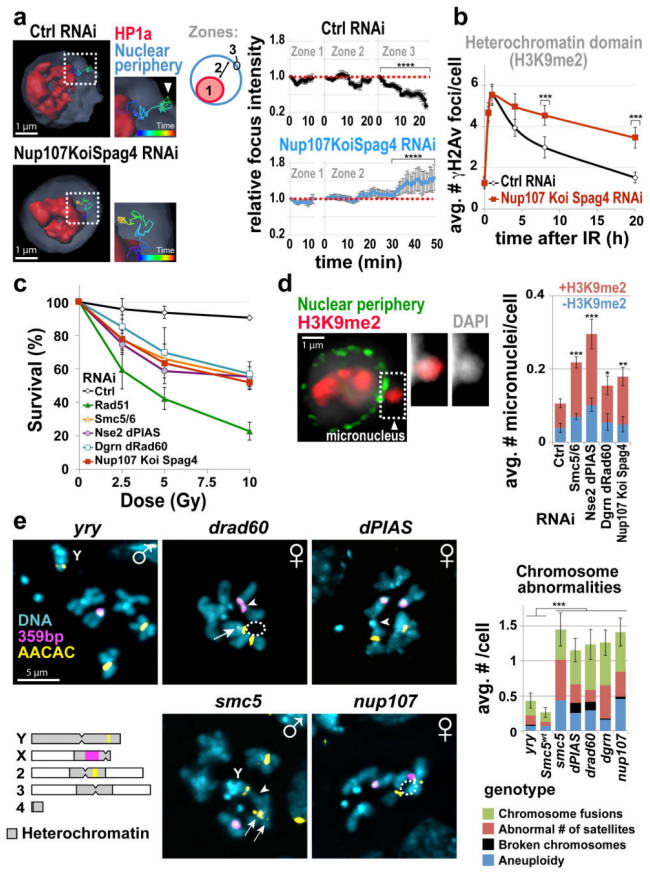

Figure 6. Relocalization is required for heterochromatin repair and stability

(**a**) Live imaging and focus tracking in cells expressing mCh-LaminC/HP1a and GFP-ATRIP (Supplementary Fig. 6a), after RNAi depletions and IR treatment. 3D reconstructions (left) show trajectory and duration of ATRIP foci leaving the heterochromatin domain (mCh-HP1a). Focus intensity quantifications (right) show changes relative to initial intensity (dashed red line) inside the heterochromatin domain (Zone 1), during relocalization (Zone 2), and at the nuclear periphery (Zone 3, mCh-LaminC) (error bars: s.e.m., ****p < 0.0001, extra sum-of-squares F-test, nonlinear regression for curve-fitting, n = 10 foci/RNAi from one experiment).

(**b**) Quantitation of cells fixed before and after IR and processed for IF, shows numbers of γH2Av foci associated with the H3K9me2 domain after RNAi depletions (error bars: s.e.m., ***p < 0.002 for Nup107+Koi+Spag4 vs. Ctrl RNAi, two-tailed Mann-Whitney test, n > 48 cells/timepoint/RNAi from one experiment).

(**c**) IR-sensitivity assay shows cell survival after RNAi depletions (see also Supplementary Fig. 6d), with Rad51 RNAi as positive control[69] (p < 0.0001 for all comparisons vs Ctrl, extra sum-of-squares F-test, nonlinear regression for curve-fitting, n > 600 cells/RNAi/dose).

(**d**) IF analysis of micronuclei (left, Smc5/6 RNAi) and quantitation (right) of cells stained for DNA (DAPI), heterochromatin (H3K9me2), and nuclear periphery (Nup107/Nup153), after RNAi depletions and IR treatment (data before IR are in Supplementary Fig. 6e). (*p <

0.05, **p < 0.01, ***p < 0.001, two tailed Mann-Whitney test, n > 190 cells/RNAi). +/− H3K9me2: micronuclei with/without H3K9me2 signals.

(**e**) Images (left) and quantitation (right) of chromosome preparations from larval neuroblasts processed for AACAC/359bp satellite FISH show chromosome abnormalities in mutants vs. controls (error bars: s.e.m., ***p < 0.001, two tailed Mann-Whitney test, n > 40 karyotypes/genotype from at least two independent crosses). Images show extra satellites (arrows), centromeric/pericentromeric fusions (*dRad60/smc5*, arrowheads), 4th-2nd chromosome fusion (*dPIAS*, arrowhead), chromosome arm losses (dashed circles). The diagram of *Drosophila* chromosomes indicates satellite positions. Protein levels for s*mc5* alleles are in Supplementary Fig. 6f.

Ctrl = control. Images in (d,e) are maximum intensity projections of Z-stacks. In (c,d), error bars represent mean +/− s.d. from three independent experiments, whereas the sample size used to determine p values is the number of cells pooled across the three experiments. Exact n values are in Supplementary Table 1.

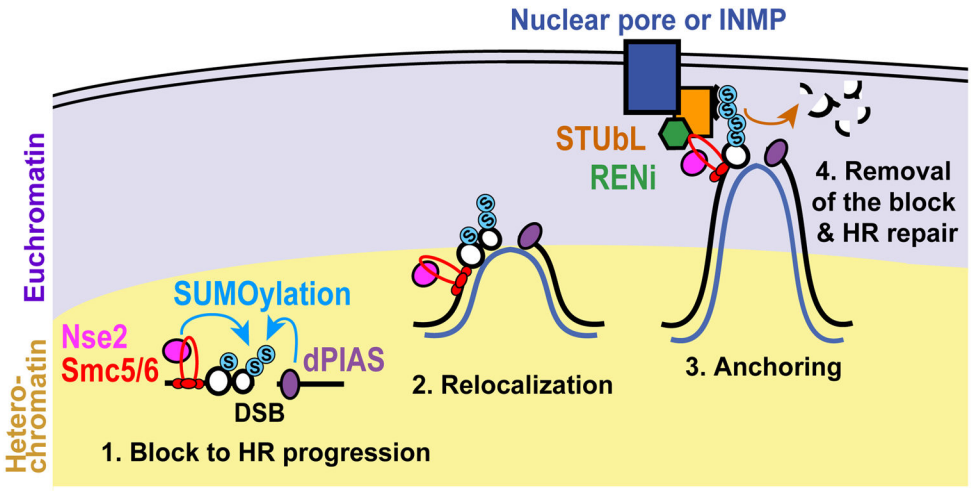

Figure 7. A model for the role of SUMOylation and the nuclear periphery in the spatial and temporal regulation of HR repair in heterochromatin

Nse2 and dPIAS-mediated SUMOylation generates a block to HR progression (*i.e.*, Rad51 recruitment) within the heterochromatin domain to prevent ectopic recombination. In addition, SUMOylation triggers the relocalization of repair sites to either INMPs or nuclear pores, where Smc5/6 interacts with the STUbL/RENi complex Dgrn/dRad60 to stabilize the association of repair sites with the nuclear periphery. Next, STUbL ubiquitylates SUMOylated proteins, enabling Rad51 recruitment and HR progression. Ubiquitylation might trigger protein degradation (as shown) or association with other repair components (not shown). This mechanism prevents ectopic recombination by isolating the damaged site from the undamaged heterochromatic repeats before strand invasion. Homolog and sister chromosome pairing is maintained during relocalization (notably homologous chromosomes display interphase pairing in *Drosophila*[70]), providing templates (blue line) for error-free HR repair.